JGP Journal of General Physiology

RESEARCH ARTICLE

Mechanism of modulation of AMPA receptors by TARP-γ8

Elisa Carrillo[1*], Sana A. Shaikh[1*], Vladimir Berka[1], Ryan J. Durham[1,2], Douglas B. Litwin[1,2], Garam Lee[1], David M. MacLean[3], Linda M. Nowak[4], and Vasanthi Jayaraman[1,2]

Fast excitatory synaptic transmission in the mammalian central nervous system is mediated by glutamate-activated α-amino-5-methyl-3-hydroxy-4-isoxazole propionate (AMPA) receptors. In neurons, AMPA receptors coassemble with transmembrane AMPA receptor regulatory proteins (TARPs). Assembly with TARP γ8 alters the biophysical properties of the receptor, producing resensitization currents in the continued presence of glutamate. Using single-channel recordings, we show that under resensitizing conditions, GluA2 AMPA receptors primarily transition to higher conductance levels, similar to activation of the receptors in the presence of cyclothiazide, which stabilizes the open state. To study the conformation associated with these states, we have used single-molecule FRET and show that this high-conductance state exhibits tighter coupling between subunits in the extracellular parts of the receptor. Furthermore, the dwell times for the transition from the tightly coupled state to the decoupled states correlate to longer open durations of the channels, thus correlating conformation and function at the single-molecule level.

Introduction

The α-amino-5-methyl-3-hydroxy-4-isoxazole propionate (AMPA) receptor is a postsynaptic ionotropic glutamate receptor that mediates and shapes fast excitatory synaptic transmission. AMPA receptors are made up of four subunits, GluA1–GluA4, that can assemble and function as homomeric and heteromeric receptors (Dingledine et al., 1999; Traynelis et al., 2010). Changes in the number and subtype of receptors provide a wide range of diversity in biophysical and pharmacological properties and underlie many forms of synaptic plasticity (Malinow and Malenka, 2002; Shepherd and Huganir, 2007; Greger et al., 2017; Diering and Huganir, 2018). Additional diversity in AMPA receptor signaling is mediated through these receptors' association with auxiliary subunits that modulate trafficking and biophysical properties of the receptors to varying degrees (Fukata et al., 2005; Milstein and Nicoll, 2008; Diering and Huganir, 2018). Among the auxiliary proteins that associate with the AMPA receptor are the transmembrane AMPA receptor regulatory proteins (TARPs). The properties of AMPA receptors coassembled with TARPs in recombinant systems closely mimic those of native AMPA receptors (Tomita et al., 2005; Kato et al., 2010b). Given the important roles these receptors play in synaptic signaling, it is essential to gain a comprehensive understanding of the functional changes associated with TARP–AMPA receptor coassembly and the conformational correlates to these functional states.

A number of investigations have focused on the structure and mechanism of modulation of AMPA receptors with the TARP stargazin, also known as γ2 (Cho et al., 2007; Tomita et al., 2005; MacLean and Bowie, 2011; MacLean et al., 2014; Cais et al., 2014; Zhang et al., 2014; Carbone and Plested, 2016; Shaikh et al., 2016; Twomey et al., 2016; Zhao et al., 2016; Coombs et al., 2017; Ben-Yaacov et al., 2017; Twomey et al., 2017; Baranovic and Plested, 2018). These studies show that γ2 interacts with the lower lobe of the ligand-binding domain (LBD) and the preM1 linker via an electrostatic patch, which may stabilize closed cleft states of the LBD, enhancing agonist efficacy. Much less is known in terms of the modulatory mechanism of the other members of the TARP family. Of particular interest is the modulation in the presence of TARPs such as γ4, γ7, and γ8, where the receptor exhibits resensitization during the longer millisecond to second timescales in the continued presence of glutamate (Kato et al., 2010a). This resensitization is characterized by an increase in

[1]Center for Membrane Biology, Department of Biochemistry and Molecular Biology, University of Texas Health Science Center at Houston, Houston, TX; [2]MD Anderson Cancer Center UTHealth Graduate School of Biomedical Sciences, University of Texas Health Science Center at Houston, Houston, TX; [3]Department of Pharmacology and Physiology, University of Rochester Medical Center, Rochester, NY; [4]Department of Molecular Medicine, Cornell University, Ithaca, NY; *E. Carrillo and S.A. Shaikh contributed equally to this work and are listed in alphabetical order.

Correspondence to Vasanthi Jayaraman: vasanthi.jayaraman@uth.tmc.edu.

https://doi.org/10.1085/jgp.201912451

steady-state current of the receptor beyond the initial desensitization in the continued presence of glutamate, where the receptor shifts from a desensitized state back to the open state (Kato et al., 2010b). The resensitization property of the TARP γ8 along with its higher expression levels in the forebrain has proved to be extremely useful in selectively inhibiting forebrain neuronal excitability in epilepsy (Kato et al., 2016; Lee et al., 2017). Specifically, compounds such as LY3130481 and JNJ 55511118 have been shown to selectively block AMPA receptors associated with the TARP γ8, with very little effect on AMPA receptors in isolation or in complex with other TARPs, thus making them excellent candidate drugs for epilepsy (Kato et al., 2016; Lee et al., 2017; Maher et al., 2016). Although these studies indicate that AMPA receptors must populate unique conformational states when in complex with the TARP γ8, which then allows for selective inhibition, what these states are and how they can be correlated to function are still largely unknown.

Using chimeras, Riva et al. (2017) were able to narrow down the region necessary for mediating the resensitization property to the second extracellular domain of the TARP γ8. On the basis of these functional data and existing structures, it is clear that the interactions at the extracellular domains are critical for mediating the modulatory properties of γ8. This interaction has recently been confirmed by the competitive antagonist 2,3-dihydroxy-6-nitro-7-sulfamoyl-benzo[f]quinoxaline (NBQX)-bound structure of the GluA2/GluA1 heteromeric receptor in complex with γ8 (Herguedas et al., 2019). However, there is currently no structure of the receptor in complex with γ8 in the presence of glutamate; hence, the underlying mechanism of resensitization is still largely unknown.

The structures of the AMPA receptors show that in the desensitized state, the receptor exhibits varying degrees of decoupling across the dimers at the amino-terminal domain (ATD) as well as within the dimer at the LBD (Dürr et al., 2014; Meyerson et al., 2014; Yelshanskaya et al., 2014). Conversely, both functional and structural studies show that stabilizing the dimer at the LBD with drugs such as cyclothiazide (CTZ) or the GluA2-L483Y mutation results in stabilizing the receptor in an open-channel state (Zhang et al., 2017; Stern-Bach et al., 1998; Sun et al., 2002; Gonzalez et al., 2010). Given that the ATD dimer–dimer interface as well as the interactions within the dimer in the LBD are critical in activation, we focused on investigating the conformational landscape in these regions to determine the mechanism underlying the resensitized state stabilized by γ8 interactions with the homomeric GluA2 AMPA receptor.

Single-molecule methods provide a window to the conformational landscape of the protein and hence yield a more comprehensive understanding of the states the protein explores (Dolino et al., 2015, 2016, 2017; Landes et al., 2011; Shaikh et al., 2016). Single-channel recordings for the AMPA receptors show a stepwise activation, with an increase in conductance level as each glutamate binds to each subunit within the tetrameric receptor (Rosenmund et al., 1998). Here we have used single-channel current recordings and single-molecule FRET (smFRET) to study the functional and conformational landscape of the receptor in the presence and absence of γ8 under apo (ligand-free) conditions, under agonist-bound conditions, and under conditions stabilizing the open-channel activated state of the receptor. Through these studies, we were able to correlate the functional properties to the conformational states and provide insight into the conformations and mechanisms underlying resensitization in AMPA receptors complexed with γ8.

Materials and methods

Cloning and mutagenesis

To generate a cysteine-light AMPA receptor for smFRET, we mutated the cysteine residues 89, 196, and 436 to serines in the GluA2-flip (unedited Q isoform) construct to obtain the cysteine-light GluA2 construct. For the measurement of intersubunit distance changes in the ATD of the AMPA receptor, a cysteine at position 23 was introduced in the cysteine-light GluA2 construct. This construct allows measurement across the dimers between the proximal B and D subunits at the ATD. For measurement of distances within the dimer, a cysteine was introduced at position 467 to measure the distance between the proximal A and D subunits at the LBD. These sites were chosen because they report on the specific distance being measured and because all other distances in the homomeric receptors are much longer and do not exhibit significant FRET. To investigate the effect of auxiliary protein γ8 on the AMPA receptor, we generated tandem constructs of the cysteine-light GluA2 mutants with γ8 in which the carboxy-terminus of GluA2 was appended to the amino-terminus of γ8 by a Gly–Ser linker using Gibson assembly. All mutagenesis was performed using standard site-directed mutagenesis procedures, and resulting constructs were analyzed by sequencing.

Functional characterization of the AMPA receptor constructs used for the smFRET experiments

We transfected HEK293 tsA201 cells at 40–50% confluency using Lipofectamine 2000 (Invitrogen) following the manufacturer's instructions with the relevant smFRET cysteine-light GluA2 or GluA2/γ8 tandem construct, and enhanced GFP DNA at a mass ratio of 1:0.5 µg per 2 ml of media. For whole-cell recordings, cells were replated after 4–6 h at a low density in fresh media containing 30 µM NBQX. Whole-cell patch-clamp recordings were performed 24–48 h after transfection using 3–5 mΩ resistance fire-polished borosilicate glass pipettes filled with the following internal solution: 135 mM CsF, 33 mM CsCl, 2 mM $MgCl_2$, 1 mM $CaCl_2$, 11 mM EGTA, and 10 mM HEPES, pH 7.4. The external solution was as follows: 150 mM NaCl, 1 mM $CaCl_2$, and 10 mM HEPES, pH 7.4. Solutions with no added ligand, 10 mM glutamate, and 10 mM glutamate with 100 µM CTZ were locally applied to lifted cells using a stepper motor system (SF-77B; Warner Instruments) with triple-barrel tubing. Recordings were performed using an Axopatch 200B amplifier (Molecular Devices) at −60-mV hold potential, acquired at 10 kHz using pCLAMP10 software (Molecular Devices), and filtered online at 5 kHz. Resensitization was quantified as the percentage of the ratio of the steady-state current to the initial peak current response evoked by the application of 10 mM glutamate.

Single-channel recordings

Recordings were performed on cells (cell-attached mode) transfected with GluA2 WT and GluA2 WT/γ8, cotransfected with GFP at a microgram ratio of 1:1, 8–24 h after transfection. Pipettes with 8–15 MΩ resistance were filled with 150 mM NaCl, 1 mM $CaCl_2$, 10 mM HEPES, and 10 mM glutamate or 10 mM glutamate with 100 µM CTZ. Data were acquired at 50 kHz and low-pass filtered at 5–10 kHz (Axon 200B and Digidata 1550A; Molecular Devices). Pipette holding potential was 100 mV. Data were further filtered at 1 kHz (Shelley et al., 2012). All recordings were idealized using the segmental k-means algorithm of QuB (Qin, 2004; Nicolai and Sachs, 2013). Given the high conductance and high probability of opening in the presence of CTZ and TARP γ8, recordings with a single highest conductance level were used as a measure to ensure that the recordings were from single channels.

The kinetic model used three closed and two open levels. After the idealized recording was visually inspected and noise spikes were removed, open and shut times were exported to the Channel Lab program (Synaptosoft), and histograms of the dwell times were displayed and fitted with log-likelihood log-binned subroutines (Zhang et al., 2017). The mean open time, mean shut time, and open probability were obtained using Channel Lab with an imposed dead time of 100 µs. Bursts of openings were defined as activations separated by shut times shorter than t_{crit} of 2–5 ms, which were calculated from the shut-time distribution (Colquhoun and Sigworth, 1995).

The conductance levels obtained from the idealized data were used to generate the transition occurrence maps. Briefly, the number of times each possible transition from one conductance level to another occurred was counted. This process was repeated for several representative traces from each condition. The number of each state-to-state transition under a given condition was then divided by the total recording length of the traces used to observe those transitions. Then, the occurrence of each transition was used to build a left matrix for each condition with state-to-itself transitions along the diagonal fixed to zero. The matrices obtained in this way were then used to generate 3-D surface plots in Origin (OriginLab Corp.).

smFRET measurements

HEK293T cells were transfected using the manufacturer's protocol for jetPRIME (Polyplus-transfection) with 3 µg of DNA and grown in media containing 30 µM NBQX. The cells were harvested after 48 h and washed with extracellular buffer (160 mM NaCl, 1.8 mM $MgCl_2$, 1 mM $CaCl_2$, 3 mM KCl, 10 mM glucose, and 10 mM HEPES, pH 7.4). The cells were then labeled with 300 nM each of maleimide derivatives of Alexa Fluor 555 donor and Alexa Fluor 647 acceptor fluorophores (Invitrogen). After being washed to remove excess fluorophores, the cells were solubilized by nutating in the dark for 1 h in chilled PBS containing 10 mM lauryl maltose neopentyl glycol and 0.25 mM cholesteryl hemisuccinate with protease inhibitor (Thermo Fisher Scientific). The lysed cells were centrifuged at 100,000×*g* at 4°C for 1 h, and the supernatant was used for smFRET sample preparation. Slides for smFRET studies were prepared and measurements taken as described previously (Dolino et al., 2015; Litwin et al., 2019). A 1-ms resolution was used to acquire the photon counts produced per donor and acceptor excitation, then binned to 5 ms and denoised with wavelet decomposition (Taylor et al., 2010; Taylor and Landes, 2011). The background-corrected signal was used to calculate the FRET efficiency using the equation:

$$E_A = \frac{I_A}{I_A + I_D}, \quad (1)$$

where E_A is the apparent FRET efficiency, I_A is the background-corrected acceptor fluorescence intensity, and I_D is the background-corrected donor fluorescence intensity. Step transition and state identification analysis was used to determine the ideal number of states for the distribution of FRET efficiencies found in the obtained FRET data (Shuang et al., 2014). Observed efficiency histograms were fit to Gaussian distributions. Distance was determined from the FRET efficiencies using the Förster equation:

$$E = \left(1 + \left[\left(\frac{R}{R_0}\right)^6\right]\right)^{-1}, \quad (2)$$

where R is the distance between the dyes and R_0 is the distance at half-maximal efficiency. The R_0 is 51 Å for the Alexa Fluor 555–Alexa Fluor 647 fluorophore pair used for these experiments.

Dwell times

The denoised traces were analyzed using hidden Markov analysis software (HaMMy; McKinney et al., 2006) to obtain state transitions and dwell times. The dwell-time distributions were then plotted using Origin and fit to an exponential decay function to determine the lifetimes. Because of experimental constraints related to fluorophore photobleaching and data binning, only dwell times longer than 5 ms and shorter than a few seconds can be detected.

Statistics

All electrophysiological data were statistically analyzed using one-way ANOVA followed by pairwise comparisons using Bonferroni's multiple comparisons test. These tests were performed using GraphPad Prism software (GraphPad Software). For all tests, $P < 0.05$ was considered significant. The number of patches used was six for WT, four for GluA2 in the presence of glutamate and CTZ, and six for GluA2 in the presence of glutamate and γ8.

For smFRET, data were analyzed using Origin 9.0 (OriginLab Corp.), MATLAB (MathWorks), and Excel (Microsoft Corp.). At least two experiments were performed for each of the conditions. The numbers of molecules used for the histograms for D23C Apo, D23C/γ8 apo, D23C/γ8 glutamate, L467C apo, L467C glutamate, L467C glutamate + CTZ, L467C/γ8 apo, and L467C/γ8 glutamate were 37, 35, 36, 37, 36, 30, 42, and 51, respectively.

Online supplemental material

Fig. S1 shows additional single-channel traces for GluA2 and GluA2 in the presence of glutamate and CTZ, and for GluA2 in the presence of glutamate and γ8. Fig. S2 shows whole-cell recordings provided for D23C and L467C mutants with and

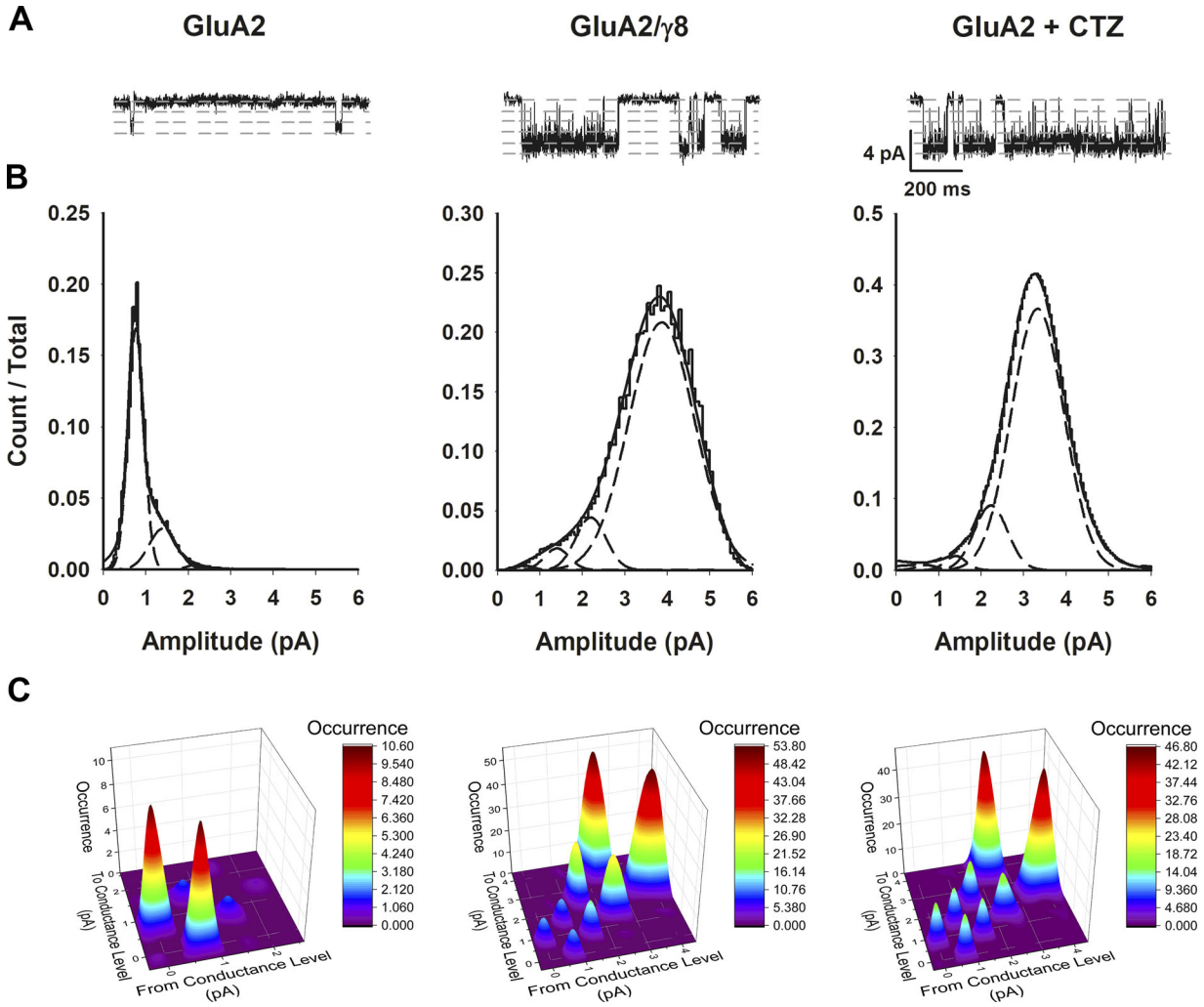

Figure 1. **γ8 induces a GluA2 receptor subconductance landscape similar to that in the presence of CTZ. (A)** Single-channel currents recorded from GluA2 WT homomeric receptor alone, as the tandem construct with γ8, and in the presence of 100 µM CTZ during continuous application of 10 mM glutamate. Openings are shown as downward deflections. **(B)** Amplitude histograms of single-channel events from patches fitted with two Gaussian components. **(C)** Maps of the transitions between conductance levels.

without γ8 (tandem) and compared with those of WT receptors, and percentage resensitization due to γ8 is shown from at least three cells. These data show that the modified receptors used in smFRET experiments demonstrate function similar to that of the WT receptor. Fig. S3 shows representative smFRET trace at the donor and acceptor emission wavelength showing a single photobleaching step and anticorrelation.

Results

Functional landscape studies by single-channel recordings

Example traces of single-channel currents activated by 10 mM glutamate in cell-attached patch recordings from cells expressing GluA2 homomeric receptors are shown in Fig. 1 A. The single-channel current recordings for the GluA2 homomeric receptor show primarily closed states with brief openings primarily to the low-amplitude subconductance levels (Fig. 1, A and B, Fig. S1, and Table 1). The low probability of opening (Fig. 2) is consistent with nearly complete desensitization observed in the presence of 10 mM glutamate (Fig. S2). Additionally, a stepwise transition to the next higher/lower conductance level is observed, as seen in the transition probability maps obtained from the single-channel traces (Fig. 1 C). These results are consistent with those previously reported for the homomeric AMPA receptors (Shelley et al., 2012; Zhang et al., 2017).

The single-channel currents for GluA2/γ8 receptors 10 mM glutamate, however, show primarily a population of the high-conductance states (Fig. 1, A and B, Fig. S1, and Table 1) and opening to the two highest conductance levels, as seen from the transition maps (Fig. 1 C). In addition to populating the higher conductance level, the probability of opening is also higher (0.42 ± 0.08) for GluA2/γ8 receptors (Fig. 2). This higher probability of opening is consistent with resensitization observed for the GluA2/γ8 receptors in the continued presence of 10 mM glutamate (Fig. S2; Carbone and Plested, 2016).

Given that resensitization leads to an increase in channel-opening events in GluA2/γ8 receptors, we also studied the gating properties of GluA2 receptors under conditions stabilizing

Table 1. **Conductance levels, open-time events, and shut-time events for GluA2 receptor alone, in tandem with γ8, and in the presence of CTZ**

Conductance level (pS)	GluA2	GluA2/γ8	GluA2 + CTZ
1	7.0 ± 0.4 (71.0 ± 2.0%)	7.0 ± 1.0 (3.5 ± 0.5%)[a]	7.0 ± 0.5 (4.5 ± 0.25%)[a]
2	14.0 ± 1.9 (21.0 ± 2.0%)	14.0 ± 0.8 (10.5 ± 1%)[a]	14.0 ± 0.5 (12.5 ± 0.6%)[a]
3	22.0 ± 0.9 (3.5 ± 1.1%)	22.0 ± 1.4 (16.0 ± 4.0%)[a]	22.0 ± 1.7 (19.0 ± 9.0%)[a]
4	—	37.0 ± 1.5 (75.0 ± 12.0%)	37.0 ± 2.1 (72.0 ± 10.0%)
Mean open period (ms)	2.0 ± 0.4	17.0 ± 1.6[b]	31.4 ± 1.6[a]
Open events			
τ1	1.0 ± 0.3 (89.0 ± 3.0%)	0.8 ± 0.1 (78.0 ± 11.0%)	0.5 ± 0.15 (20 ± 6.0%)
τ2	8.2 ± 2.2 (10.0 ± 2.0%)	9.0 ± 5.0 (13.0 ± 5.0%)	38.0 ± 5.0 (80.0 ± 13%)
τ3	—	81.0 ± 16.0 (9.0 ± 4.0%)	—
Mean shut period (ms)	479.0 ± 57.0	36.8 ± 10.5[a]	10.3 ± 0.7[a]
Shut events			
τ1	5.6 ± 0.3 (27.2 ± 4.1%)	0.7 ± 0.3 (70 ± 10.0%)	0.7 ± 0.1 (49.2 ± 4.5%)
τ2	203.5 ± 14.0 (50.0 ± 9.0%)	4.6 ± 1.4 (15 ± 5.0%)	5.0 ± 1.0 (34.2 ± 7.6%)
τ3	1,093.0 ± 162.0 (22.0 ± 5.0%)	60.0 ± 10.0 (11.0 ± 7.0%)	48.0 ± 5.0 (16.6 ± 3.6%)
τ4	—	527.0 ± 183.0 (5.0 ± 3.0%)	—

Percentage of occurrence for each level or event is shown next to its value in parentheses. The error in the lifetimes is the SE of the fit. The table is related to Figs. 1 and 3.
[a]P < 0.001 compared with GluA2.
[b]P < 0.01 compared with GluA2.

the open-channel state by adding 100 µM CTZ. The single-channel traces again show primarily a population of the high conductance levels (Fig. 1, A and B, Fig. S1, and Table 1), and similar to what is seen for GluA2/γ8 receptors, the transitions are mainly from the closed state to the higher conductance levels (Fig. 1 C). Because CTZ stabilizes the open-channel state, the probability of opening (0.74 ± 0.004) is high (Fig. 2). This is again consistent with the whole-cell currents recorded under saturating concentrations of glutamate in the presence of CTZ.

To characterize the kinetics, we constructed dwell-time distributions of open and closed events and fitted these with multiple component exponentials (Fig. 3). We did not separate the events on the basis of conductance, because the receptors under the conditions being studied had a significant fraction in the highest conductance level. The open time events for the GluA2 homomeric receptor in the presence of 10 mM glutamate and 100 µM CTZ and the GluA2/γ8 receptors in the presence of 10 mM glutamate could be fit to both short- and long-lived states (Fig. 3 A and Table 1). The difference between GluA2 receptors in the presence of CTZ and GluA2/γ8 receptors is that GluA2 in the presence of CTZ primarily (80%) exhibited openings that could be fit to a lifetime of 38 ms, whereas GluA2/γ8 receptors have primarily brief events, with 78% of events that had a lifetime of <1 ms and 10% being longer than that observed for CTZ with a lifetime of 81 ms (Table 1). The closed time histograms also show differences between the two conditions (Fig. 3 B and Table 1), with the GluA2/γ8 receptors exhibiting 70% short closed lifetimes of <1 ms compared with 49% in the case of GluA2 receptors in the presence of CTZ. Additionally, a small fraction of the GluA2/γ8 receptors exhibited the very long closed time of 527 ms, whereas the longest-lived states for GluA2 receptors in the presence and absence of CTZ had a lifetime of 48 ms (Table 1).

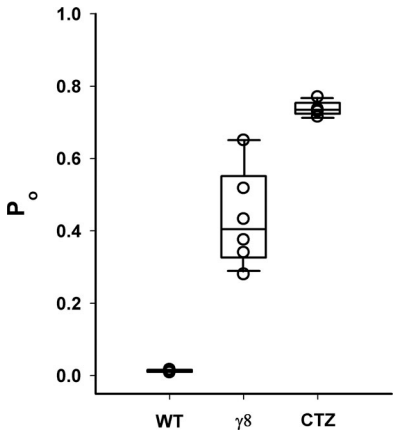

Figure 2. **Open probability of GluA2 receptors.** Open probability (P_o) of GluA2 receptors in the absence of CTZ, in tandem with γ8, and in the presence of CTZ. Error bars are SEM.

To correlate these functional properties of GluA2 receptors to conformations, we probed the changes at the interfaces of the ATD and LBD that have previously been shown to be sites of large changes (Meyerson et al., 2014; Gonzalez et al., 2010) during activation and desensitization using smFRET measurements.

Conformational landscape at the dimer–dimer interface of the ATD

To study the conformational landscape at the ATD of the GluA2 receptor in the presence and absence of γ8, we have used a

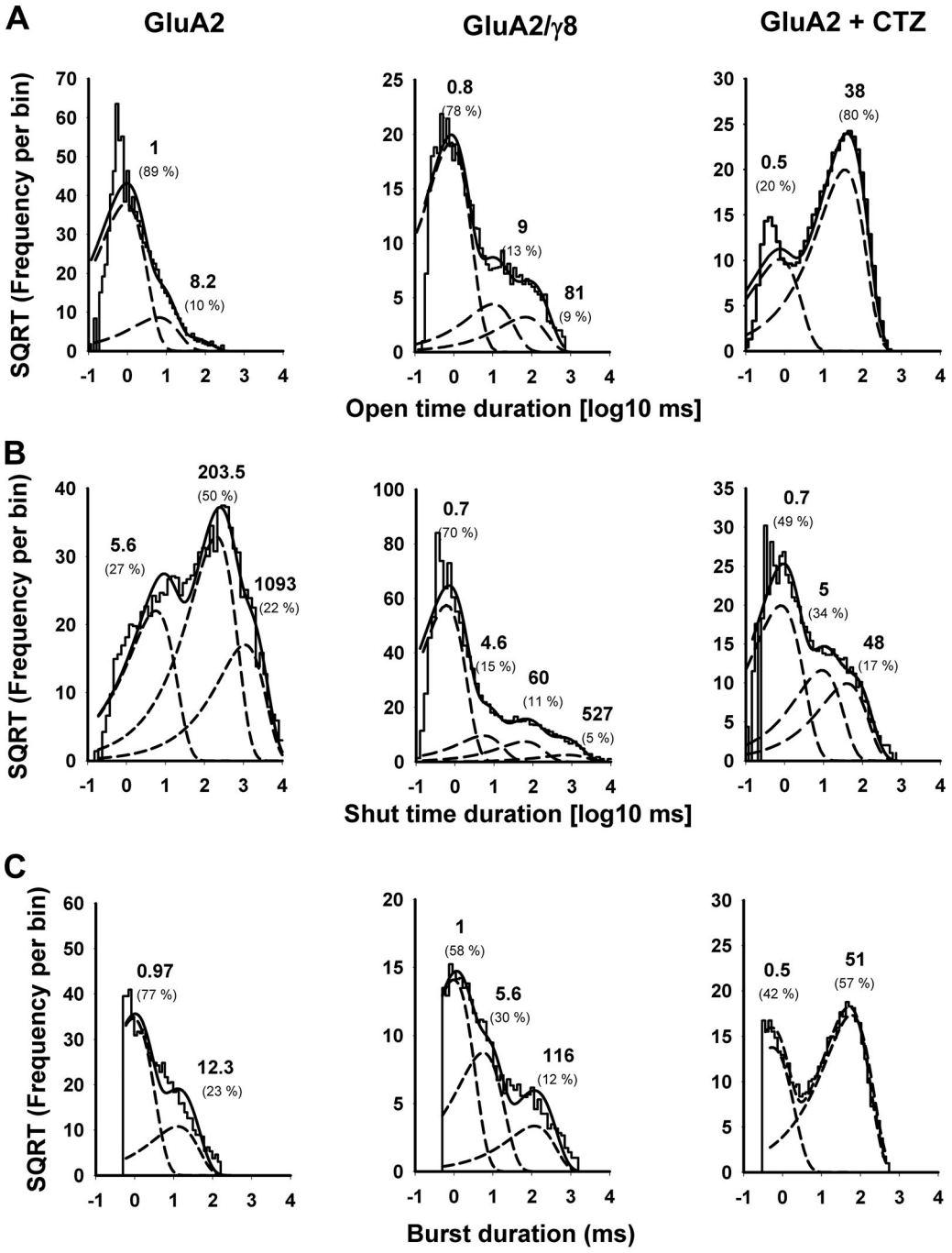

Figure 3. **Dwell-time distribution of GluA2 receptors from single-channel recordings. (A)** Open time. **(B)** Shut time. **(C)** Burst duration dwell-time distributions for GluA2 receptor alone, in GluA2/γ8, and in GluA2 in the presence of CTZ, with 10 mM glutamate. SQRT, square root.

cysteine-light GluA2 receptor and introduced cysteine at site 23. This site is ideal for probing the conformational decoupling across the dimer–dimer interface at the ATD (Fig. 4). The modified smFRET construct exhibits properties similar to those of the WT GluA2 receptor and also has resensitization properties in the presence of γ8 similar to those observed for the WT receptor (Fig. S2). For the smFRET measurements, only traces exhibiting single photobleaching steps for the donor and acceptor with anticorrelation between the two were chosen (Fig. S3). Representative smFRET traces in the FRETing region, along with the normalized FRET efficiency histogram for the GluA2 receptor D23C mutant in the ligand-free (apo), glutamate and CTZ-bound (open) states (Shaikh et al., 2016) and the glutamate-bound (desensitized) state (Shaikh et al., 2016) are shown in Fig. 4, A–C, and the corresponding traces and efficiency histograms for the GluA2/γ8 receptors are shown in Fig. 4, D and E.

The smFRET efficiency histograms show that in the apo state, the GluA2 receptor as well as the GluA2/γ8 receptors exhibit

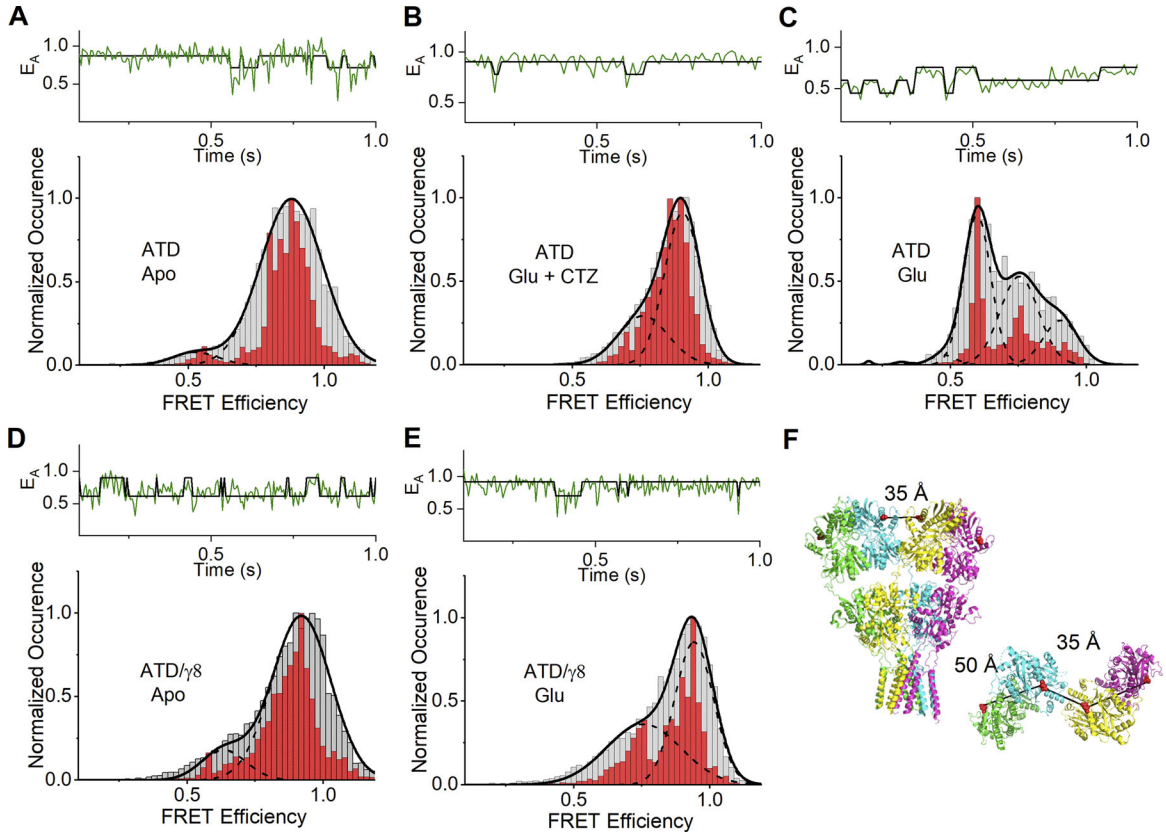

Figure 4. **Conformational landscape at the ATD of the GluA2 receptor. (A–E)** smFRET histograms for site 23 of the GluA2 receptor under (A) unliganded apo condition, (B) open condition (in the presence of 1 mM glutamate + 100 µM CTZ), (C) desensitized condition (in the presence of 1 mM glutamate), (D) in tandem with γ8 in unliganded apo condition, and (E) in tandem with γ8 in the desensitized condition (in the presence of 1 mM glutamate). Corresponding representative smFRET traces are shown above each histogram. Denoised smFRET histograms are in red, and observed histograms with Gaussian fits are in gray. **(F)** Fluorophore attachment site 23 at the ATD of GluA2 receptors shown in the side view and top view of full-length GluA2 receptor (PDB accession no. 4U2P; apo).

profiles similar to those of the receptor existing primarily in high FRET states 0.88 ± 0.01 and 0.92 ± 0.01 efficiency, corresponding to distances of 37 ± 0.5 Å and 34 ± 0.8 Å, respectively (Table 2). A smaller fraction is observed at FRET efficiencies of 0.53 ± 0.02 and 0.64 ± 0.02, which correspond to distances of 50 ± 0.7 Å and 46 ± 0.7 Å, respectively. These distances correlate well with the distances within and across the dimer in the known apo state structures of AMPA with distances of 35 Å and 50 Å, respectively (PDB accession no. 4U2P). Given the similarities in the smFRET histograms for the apo state of the GluA2 receptor as well as the GluA2/γ8 receptors, we can conclude that the conformational landscape at the dimer–dimer interface is not significantly altered due to the presence of γ8 in the apo resting state of the GluA2 receptor.

Comparing the smFRET efficiency histogram for the glutamate-bound form of the GluA2/γ8 receptors with that of the previously reported data for GluA2 receptors bound to glutamate in the presence of CTZ, it is clear that the two have similar high FRET efficiency states at 0.94 ± 0.01 and 0.90 ± 0.01, respectively. Additionally, glutamate-bound forms of both GluA2/γ8 receptors and GluA2 receptors show a lower efficiency state. This low-efficiency FRET state could correspond to the fraction of the receptors in a desensitized state. This assignment is consistent with previously published data showing minimal high FRET efficiency states in GluA2 receptors bound to glutamate where the receptor is primarily in the desensitized state (Fig. 4 C; Shaikh et al., 2016). The assignment of the high FRET state to an open-channel state is further validated by the correlation between the percentages in this state with single-channel recording: 55% of the glutamate-bound form of GluA2/γ8 receptors and 70% of GluA2 receptors in the presence of CTZ are in the high FRET state in the smFRET data. This is similar to the open-channel fractions of 0.42 and 0.74 determined from the single-channel recordings.

The dwell times for the transitions from the high FRET state to the low FRET state (decoupling of the interface) and from the low FRET state to the high FRET state (coupling of the interface) are shown in Fig. 5. The data for all transitions could be fit with a single exponential decay. The lifetimes for the transition from the coupled to decoupled state of 40 ± 5 ms and 68 ± 14 ms for glutamate-bound GluA2 in the presence of CTZ and glutamate-bound GluA2/γ8 receptors, respectively, are in close agreement with longer open-channel lifetimes of 38 ± 5 ms and 81 ± 16 ms determined from the single-channel recordings. Similarly, the dwell times for the reverse transition from the decoupled to coupled state can be fit to lifetimes of 42 ± 4 ms and 144 ± 59 ms

Table 2. **smFRET conformational states occupied by AMPA receptor**

Construct	State	Occupancy (%)	StaSI efficiency state	FRET distance (Å)	Gaussian state	Cα–Cα structure distance (Å) (Protein Data Bank accession no.)
AMPA receptor (D23C) apo	State 1	94.55	0.88	37 ± 0.5	0.88 ± 0.01	35 (4U2P[a])
	State 2	5.45	0.55	50 ± 0.7	0.53 ± 0.02	41 (5L1B[a])
AMPA receptor (D23C)/γ8 apo	State 1	87.72	0.89	34 ± 0.8	0.92 ± 0.01	
	State 2	12.28	0.61	46 ± 0.7	0.64 ± 0.02	
AMPA receptor (D23C) Glu + CTZ[b]	State 1	69.18	0.89	35 ± 0.7	0.90 ± 0.01	41 (4UQK[c])
	State 2	30.82	0.76	42 ± 0.8	0.76 ± 0.02	43 (6DLZ[c]) 44 (5WEO[c])
AMPA receptor (D23C) Glu[b]	State 1	17.0	0.90	34 ± 2.3	0.92 ± 0.03	33
	State 2	35.8	0.75	42 ± 0.4	0.76 ± 0.01	(4U1Y[d])
	State 3	44.4	0.60	48 ± 0.3	0.60 ± 0.01	41
	State 4	2.1	0.44	52 ± 0.7	0.46 ± 0.02	(5VHZ[d])
AMPA receptor (D23C)/γ8 Glu	State 1	54.95	0.91	32 ± 1.0	0.94 ± 0.01	
	State 2	45.05	0.70	42 ± 1.1	0.76 ± 0.03	
AMPA receptor (L467C) apo	State 1	74.41	0.90	34 ± 0.8	0.92 ± 0.01	33 (4U2P[a])
	State 2	25.59	0.68	45 ± 0.7	0.68 ± 0.02	33 (5L1B[a])
AMPA receptor (L467C)/γ8 apo	State 1	65.74	0.92	34 ± 0.8	0.92 ± 0.01	
	State 2	34.26	0.72	44 ± 0.7	0.72 ± 0.02	
AMPA receptor (L467C) Glu + CTZ	State 1	40.60	0.94	31 ± 2.1	0.95 ± 0.02	33 (4UQK[c])
	State 2	17.91	0.87	38 ± 1.0	0.86 ± 0.02	34 (6DLZ[c])
	State 3	24.34	0.77	42 ± 1.9	0.75 ± 0.05	34
	State 4	17.15	0.61	47 ± 0.3	0.61 ± 0.1	(5WEO[c])
AMPA receptor (L467C)/γ8 Glu	State 1	35.89	0.94	30 ± 2.6	0.96 ± 0.02	
	State 2	29.68	0.83	39 ± 2.4	0.84 ± 0.05	
	State 3	17.34	0.70	44 ± 2.5	0.70 ± 0.07	
	State 4	17.09	0.55	50 ± 1.3	0.52 ± 0.04	
AMPA receptor (L467C) Glu	State 1	27.32	0.89	35 ± 1.4	0.91 ± 0.02	33
	State 2	52.32	0.76	42 ± 0.8	0.77 ± 0.02	(4U1Y[d])
	State 3	16.64	0.60	48 ± 3.3	0.58 ± 0.1	40
	State 4	3.72	0.46	53 ± 3.6	0.42 ± 0.1	(5VHZ[d])

STaSI, step transition and state identification used to determine the states as stated in Materials and methods. Gaussian states were obtained from fitting the observed data.

[a]Structures 4U2P and 5L1B represent the apo structure of the receptor.

[b]Data from Shaikh et al. (2016).

[c]Structures 4UQK, 6DLZ, and 5WEO represent the open structure of the receptor.

[d]Structures 4U1Y and 5VHZ represent the desensitized structure of the receptor.

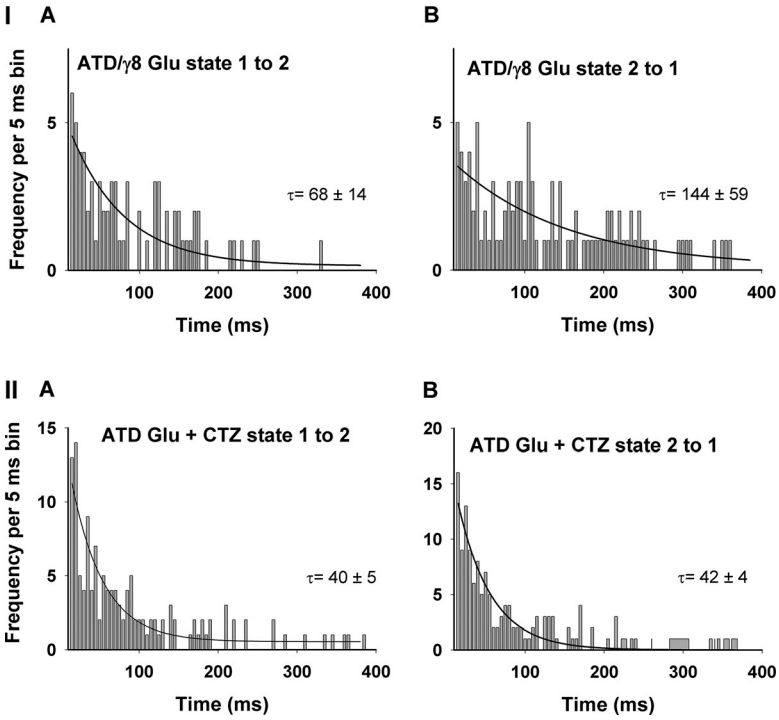

Figure 5. **Dwell-time distributions for transitions between the smFRET states at site 23. (I)** Comparison of dwell times for transitions in GluA2/γ8 and in the presence of glutamate between (A) the high FRET state 1 to the low FRET state 2 and between (B) the low FRET state 2 to the high FRET state 1. **(II)** Comparison of dwell times for transitions in GluA2 in the presence of CTZ and glutamate between (A) the high FRET state 1 and the low FRET state 2 and between (B) the low FRET state 2 and the high FRET state 1.

for glutamate-bound GluA2 in the presence of CTZ and glutamate-bound GluA2/γ8 receptors, respectively, and show trends similar to those of the longer closed-channel lifetimes of 48 ± 5 ms for glutamate-bound GluA2 in the presence of CTZ and two lifetimes of 60 ± 10 ms and 527 ± 183 ms for glutamate-bound GluA2/γ8.

Conformational landscape within the dimer interface at the LBD

To characterize the conformational landscape at the LBD, we focused on the interface within the dimer because this has been established to be a region critical in activation and desensitization of the receptor (Gonzalez et al., 2010; Sun et al., 2002). Site 467 is ideal for these measurements because it is able to differentiate distances within and across the dimers (Fig. 6). The function of the construct with cysteine at site 467 in the cysteine-light GluA2 receptor is similar to that of the WT receptor with and without γ8 (Fig. S2). Representative smFRET traces along with the normalized FRET efficiency histogram for GluA2 receptor L467C mutant and GluA2/γ8 L467C mutant receptor are shown in Fig. 6. Similar to the results at the ATD, the smFRET efficiency histograms show that in the unliganded apo state, the GluA2 receptor as well as the GluA2/γ8 receptors exhibit similar profiles, with the receptor existing primarily in a high FRET state of 0.92 ± 0.01 efficiency (Table 2).

The smFRET histograms of the glutamate-bound form of GluA2/γ8 receptors and the glutamate-bound form of the GluA2 receptor in the presence of CTZ (Fig. 6) exhibit a high efficiency state (0.96 ± 0.02 and 0.95 ± 0.02, respectively; Table 2). The smFRET histograms for GluA2 in the presence of glutamate and without CTZ show primarily larger distances, indicating a decoupling interface consistent with the protein being primarily desensitized under these conditions. The similar high FRET states for GluA2/γ8 receptors and the glutamate-bound form of the GluA2 receptor in the presence of CTZ indicate that the resensitized state of the glutamate-bound GluA2/γ8 receptors is similar at this interface to that seen in the glutamate- and CTZ-bound GluA2 receptors, albeit with a lower fraction between coupled state relative to decoupled as expected on the basis of open probabilities.

The lifetimes (Fig. 7) from the highest FRET efficiency state (0.96) to the lower FRET efficiency state (0.84) are 32 ± 3 ms for glutamate-bound GluA2 in the presence of CTZ and 74 ± 1.3 ms for glutamate-bound GluA2/γ8 receptors. These smFRET lifetimes again correspond closely to the longer open durations in single-channel recording for glutamate-bound GluA2 in the presence of CTZ (38 ± 5 ms) and glutamate-bound GluA2/γ8 (81 ± 16 ms) receptors, respectively. There are several decoupled states observed at the LBD for both glutamate-bound GluA2 in the presence of CTZ and glutamate-bound GluA2/γ8 receptors; however, the lower FRET states 3 and 4 (Table 1) had very few transitions (50 or fewer) and did not provide enough events to have statistical significance. The transitions from state 2 to state 1 could be fit to one exponential decay and had lifetimes of 37 ± 5 ms and 50 ± 10 ms for glutamate-bound GluA2 in the presence of CTZ and glutamate-bound GluA2/γ8 receptors, respectively. These are again similar to longer closed-channel dwell times of 48 ± 5 ms for glutamate-bound GluA2 in the presence of CTZ and 60 ± 10 ms for glutamate-bound GluA2/γ8 seen in the single-channel recordings.

The direct correlations between the first coupling/decoupling step at the LBD dimer interface for glutamate-bound GluA2/γ8 with the longer dwell time for closed-/open-channel states in the single-channel recordings further confirm the assignment that the coupling of the dimer interface at the LBD contributes to the resensitized open-channel state, and this is similar to that observed in glutamate-bound GluA2 in the presence of CTZ.

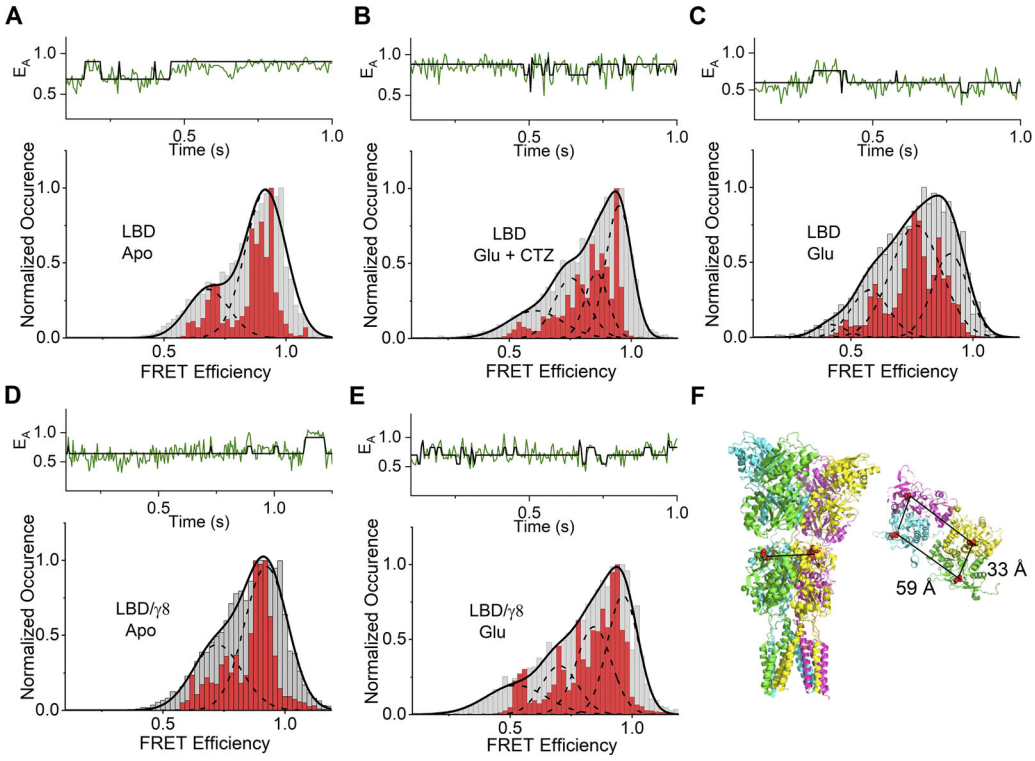

Figure 6. **Conformational landscape at the LBD of the GluA2 receptor.** smFRET histograms for site 467 of the GluA2 receptor under (A) unliganded apo condition, (B) open condition (in the presence of 1 mM glutamate + 100 µM CTZ), (C) desensitized condition (in the presence of 1 mM glutamate), (D) in tandem with γ8 in unliganded apo condition, and (E) in tandem with γ8 in the desensitized condition (in the presence of 1 mM glutamate). Corresponding representative smFRET traces are shown above each histogram. Denoised smFRET histograms are in red, and observed ligand-binding terminal domain of GluA2 receptors is shown in the side view and top view of full-length GluA2 receptor (PDB accession no. 4U2P; apo). E_A, apparent FRET efficiency.

Discussion

A large number of structures are available for the AMPA receptor in various liganded conditions, in addition to structures of the receptor in the presence of the auxiliary protein γ2 (Dürr et al., 2014; Sobolevsky et al., 2009; Yelshanskaya et al., 2014; Zhao et al., 2016; Twomey et al., 2016; Twomey et al., 2017; Chen et al., 2017; Meyerson et al., 2014). In addition, spectroscopic and biochemical investigations have provided a map of the

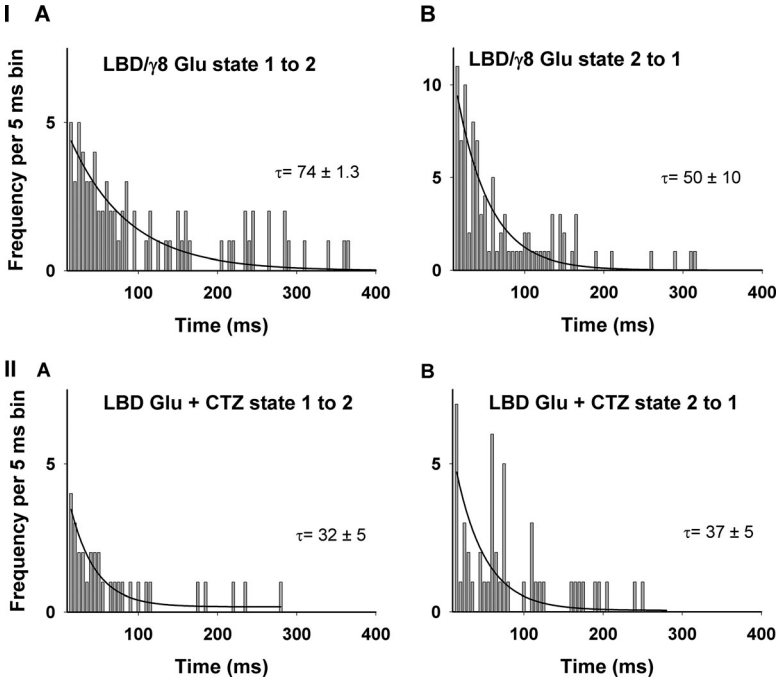

Figure 7. **Dwell time distributions for transitions between the smFRET states at site 467. (I)** Comparison of dwell times for transitions in GluA2/γ8 and in the presence of glutamate between (A) the high FRET state 1 and the low FRET state 2 and between (B) the low FRET state 2 and the high FRET state 1. **(II)** Comparison of dwell times for transitions in GluA2 in the presence of CTZ and glutamate between (A) the high FRET state 1 and the low FRET state 2 and between (B) the low FRET state 2 and the high FRET state 1.

conformational and functional landscape of the receptor under these conditions (Gonzalez et al., 2008; Gonzalez et al., 2010; Ramaswamy et al., 2012; MacLean et al., 2014). Much less is known of the modulation of the AMPA receptor by auxiliary subunit γ8 and the mechanism of resensitization that occurs in its presence. A recent structure has been published for GluA2 receptors in complex with γ8 that showed a number of similarities to prior structures of GluA2 in complex with γ2 that demonstrate extensive interactions at the transmembrane segments and at the pretransmembrane segments (Herguedas et al., 2019). This structure, however, is in the presence of competitive antagonist NBQX; hence, glutamate-induced conformational changes underlying resensitization are still unknown (Herguedas et al., 2019). Here, we have used single-channel and smFRET measurements to study the functional and conformational landscape of homomeric GluA2 receptors in the presence and absence of γ8 to gain an understanding of the functional and conformational states underlying resensitization.

The smFRET investigations presented here reveal that the conformational landscape representing the resensitized state of GluA2/γ8 receptors in the presence of 10 mM glutamate is similar to that of GluA2 with 10 mM glutamate stabilized in the open condition by CTZ, both at the dimer–dimer interface at the ATD and at the interface within the dimer in the LBD. More importantly, we show that the slower transitions at these interfaces can be directly correlated to the burst events, as observed in the single-channel recordings showing a direct correlation of conformation and function at the single-molecule level. The data also indicate that γ8 has long-range effects on the receptor, even though the cryo-EM structure shows that its interactions are primarily in the transmembrane segments and LBD. Such long-range tighter coupling has previously been observed in both smFRET experiments (Shaikh et al., 2016) and cross-linking experiments (Cais et al., 2014) of GluA2 receptors with γ2. However, the extent of coupling is larger for GluA2 receptors with γ8 than has been seen with GluA2 receptors with γ2, which in turn correlates to the differences in modulatory properties of the two, with resensitization being observed only in the presence of γ8.

Acknowledgments

Richard W. Aldrich served as editor.

This study was supported by National Institutes of Health grants R35GM122528 (V. Jayaraman), F31GM130035 (R.J. Durham), and R00 NS094761 (D.M. MacLean), American Heart Association fellowships 18POST34030189 (E. Carrillo) and 16POST30030007 (S.A. Shaikh), and the Houston Area Molecular Biophysics Program grant T32GM008280-28 (D.B. Litwin).

The authors declare no competing financial interests.

Author contributions: S.A. Shaikh, D.B. Litwin, and G. Lee made the GluA2 mutant constructs. E. Carrillo performed the electrophysiological experiments with the advice of L.M. Nowak and D.M. MacLean. E. Carrillo, L.M. Nowak, and R.J. Durham analyzed the single-channel data. S.A. Shaikh and V. Berka performed and analyzed the smFRET experiments. E. Carrillo, S.A. Shaikh, L.M. Nowak, and V. Jayaraman designed the experiments, interpreted the results, and wrote the manuscript.

Submitted: 16 July 2019
Accepted: 4 November 2019

References

Baranovic, J., and A.J.R. Plested. 2018. Auxiliary subunits keep AMPA receptors compact during activation and desensitization. *eLife.* 7:e40548. https://doi.org/10.7554/eLife.40548

Ben-Yaacov, A., M. Gillor, T. Haham, A. Parsai, M. Qneibi, and Y. Stern-Bach. 2017. Molecular mechanism of AMPA receptor modulation by TARP/stargazin. *Neuron.* 93:1126–1137.e4. https://doi.org/10.1016/j.neuron.2017.01.032

Cais, O., B. Herguedas, K. Krol, S.G. Cull-Candy, M. Farrant, and I.H. Greger. 2014. Mapping the interaction sites between AMPA receptors and TARPs reveals a role for the receptor N-terminal domain in channel gating. *Cell Reports.* 9:728–740. https://doi.org/10.1016/j.celrep.2014.09.029

Carbone, A.L., and A.J. Plested. 2016. Superactivation of AMPA receptors by auxiliary proteins. *Nat. Commun.* 7:10178. https://doi.org/10.1038/ncomms10178

Chen, S., Y. Zhao, Y. Wang, M. Shekhar, E. Tajkhorshid, and E. Gouaux. 2017. Activation and desensitization mechanism of AMPA receptor-TARP complex by cryo-EM. *Cell.* 170:1234–1246.e14. https://doi.org/10.1016/j.cell.2017.07.045

Cho, C.H., F. St-Gelais, W. Zhang, S. Tomita, and J.R. Howe. 2007. Two families of TARP isoforms that have distinct effects on the kinetic properties of AMPA receptors and synaptic currents. *Neuron.* 55:890–904. https://doi.org/10.1016/j.neuron.2007.08.024

Colquhoun, D., and F.J. Sigworth. 1995. Fitting and Statistical Analysis of Single-Channel Records. *In* Single-Channel Recording. B. Sakmann, and E. Neher, editors. Second edition. Springer, New York. pp. 483–587.

Coombs, I.D., D.M. MacLean, V. Jayaraman, M. Farrant, and S.G. Cull-Candy. 2017. Dual effects of TARP γ-2 on glutamate efficacy can account for AMPA receptor autoinactivation. *Cell Reports.* 20:1123–1135. https://doi.org/10.1016/j.celrep.2017.07.014

Diering, G.H., and R.L. Huganir. 2018. The AMPA receptor code of synaptic plasticity. *Neuron.* 100:314–329. https://doi.org/10.1016/j.neuron.2018.10.018

Dingledine, R., K. Borges, D. Bowie, and S.F. Traynelis. 1999. The glutamate receptor ion channels. *Pharmacol. Rev.* 51:7–61.

Dolino, D.M., D. Cooper, S. Ramaswamy, H. Jaurich, C.F. Landes, and V. Jayaraman. 2015. Structural dynamics of the glycine-binding domain of the *N*-methyl-D-aspartate receptor. *J. Biol. Chem.* 290:797–804. https://doi.org/10.1074/jbc.M114.605436

Dolino, D.M., S. Rezaei Adariani, S.A. Shaikh, V. Jayaraman, and H. Sanabria. 2016. Conformational selection and submillisecond dynamics of the ligand-binding domain of the *N*-methyl-D-aspartate receptor. *J. Biol. Chem.* 291:16175–16185. https://doi.org/10.1074/jbc.M116.721274

Dolino, D.M., S. Chatterjee, D.M. MacLean, C. Flatebo, L.D.C. Bishop, S.A. Shaikh, C.F. Landes, and V. Jayaraman. 2017. The structure-energy landscape of NMDA receptor gating. *Nat. Chem. Biol.* 13:1232–1238. https://doi.org/10.1038/nchembio.2487

Dürr, K.L., L. Chen, R.A. Stein, R. De Zorzi, I.M. Folea, T. Walz, H.S. Mchaourab, and E. Gouaux. 2014. Structure and dynamics of AMPA receptor GluA2 in resting, pre-open, and desensitized states. *Cell.* 158:778–792. https://doi.org/10.1016/j.cell.2014.07.023

Fukata, Y., A.V. Tzingounis, J.C. Trinidad, M. Fukata, A.L. Burlingame, R.A. Nicoll, and D.S. Bredt. 2005. Molecular constituents of neuronal AMPA receptors. *J. Cell Biol.* 169:399–404. https://doi.org/10.1083/jcb.200501121

Gonzalez, J., A. Rambhadran, M. Du, and V. Jayaraman. 2008. LRET investigations of conformational changes in the ligand binding domain of a functional AMPA receptor. *Biochemistry.* 47:10027–10032. https://doi.org/10.1021/bi800690b

Gonzalez, J., M. Du, K. Parameshwaran, V. Suppiramaniam, and V. Jayaraman. 2010. Role of dimer interface in activation and desensitization in AMPA receptors. *Proc. Natl. Acad. Sci. USA.* 107:9891–9896. https://doi.org/10.1073/pnas.0911854107

Greger, I.H., J.F. Watson, and S.G. Cull-Candy. 2017. Structural and functional architecture of AMPA-type glutamate receptors and their auxiliary proteins. *Neuron.* 94:713–730. https://doi.org/10.1016/j.neuron.2017.04.009

Herguedas, B., J.F. Watson, H. Ho, O. Cais, J. García-Nafría, and I.H. Greger. 2019. Architecture of the heteromeric GluA1/2 AMPA receptor in complex with the auxiliary subunit TARP γ8. Science. 364:eaav9011.

Kato, A.S., M.B. Gill, M.T. Ho, H. Yu, Y. Tu, E.R. Siuda, H. Wang, Y.W. Qian, E.S. Nisenbaum, S. Tomita, et al. 2010a. Hippocampal AMPA receptor gating controlled by both TARP and cornichon proteins. *Neuron.* 68: 1082–1096. https://doi.org/10.1016/j.neuron.2010.11.026

Kato, A.S., M.B. Gill, H. Yu, E.S. Nisenbaum, and D.S. Bredt. 2010b. TARPs differentially decorate AMPA receptors to specify neuropharmacology. *Trends Neurosci.* 33:241–248. https://doi.org/10.1016/j.tins.2010.02.004

Kato, A.S., K.D. Burris, K.M. Gardinier, D.L. Gernert, W.J. Porter, J. Reel, C. Ding, Y. Tu, D.A. Schober, M.R. Lee, et al. 2016. Forebrain-selective AMPA-receptor antagonism guided by TARP γ-8 as an antiepileptic mechanism. *Nat. Med.* 22:1496–1501. https://doi.org/10.1038/nm.4221

Landes, C.F., A. Rambhadran, J.N. Taylor, F. Salatan, and V. Jayaraman. 2011. Structural landscape of isolated agonist-binding domains from single AMPA receptors. *Nat. Chem. Biol.* 7:168–173. https://doi.org/10.1038/nchembio.523

Lee, M.R., K.M. Gardinier, D.L. Gernert, D.A. Schober, R.A. Wright, H. Wang, Y. Qian, J.M. Witkin, E.S. Nisenbaum, and A.S. Kato. 2017. Structural determinants of the γ-8 TARP dependent AMPA receptor antagonist. *ACS Chem. Neurosci.* 8:2631–2647. https://doi.org/10.1021/acschemneuro.7b00186

Litwin, D.B., E. Carrillo, S.A. Shaikh, V. Berka, and V. Jayaraman. 2019. The structural arrangement at intersubunit interfaces in homomeric kainate receptors. *Sci. Rep.* 9:6969. https://doi.org/10.1038/s41598-019-43360-x

MacLean, D.M., and D. Bowie. 2011. Transmembrane AMPA receptor regulatory protein regulation of competitive antagonism: a problem of interpretation. *J. Physiol.* 589:5383–5390. https://doi.org/10.1113/jphysiol.2011.219485

MacLean, D.M., S.S. Ramaswamy, M. Du, J.R. Howe, and V. Jayaraman. 2014. Stargazin promotes closure of the AMPA receptor ligand-binding domain. *J. Gen. Physiol.* 144:503–512. https://doi.org/10.1085/jgp.201411287

Maher, M.P., N. Wu, S. Ravula, M.K. Ameriks, B.M. Savall, C. Liu, B. Lord, R.M. Wyatt, J.A. Matta, C. Dugovic, et al. 2016. Discovery and characterization of AMPA receptor modulators selective for TARP-γ8. *J. Pharmacol. Exp. Ther.* 357:394–414. https://doi.org/10.1124/jpet.115.231712

Malinow, R., and R.C. Malenka. 2002. AMPA receptor trafficking and synaptic plasticity. *Annu. Rev. Neurosci.* 25:103–126. https://doi.org/10.1146/annurev.neuro.25.112701.142758

McKinney, S.A., C. Joo, and T. Ha. 2006. Analysis of single-molecule FRET trajectories using hidden Markov modeling. *Biophys. J.* 91:1941–1951. https://doi.org/10.1529/biophysj.106.082487

Meyerson, J.R., J. Kumar, S. Chittori, P. Rao, J. Pierson, A. Bartesaghi, M.L. Mayer, and S. Subramaniam. 2014. Structural mechanism of glutamate receptor activation and desensitization. *Nature.* 514:328–334. https://doi.org/10.1038/nature13603

Milstein, A.D., and R.A. Nicoll. 2008. Regulation of AMPA receptor gating and pharmacology by TARP auxiliary subunits. *Trends Pharmacol. Sci.* 29: 333–339. https://doi.org/10.1016/j.tips.2008.04.004

Nicolai, C., and F. Sachs. 2013. Solving ion channel kinetics with the QuB software. *Biophys. Rev. Lett.* 08:191–211. https://doi.org/10.1142/S1793048013300053

Qin, F. 2004. Restoration of single-channel currents using the segmental k-means method based on hidden Markov modeling. *Biophys. J.* 86: 1488–1501. https://doi.org/10.1016/S0006-3495(04)74217-4

Ramaswamy, S., D. Cooper, N. Poddar, D.M. MacLean, A. Rambhadran, J.N. Taylor, H. Uhm, C.F. Landes, and V. Jayaraman. 2012. Role of conformational dynamics in α-amino-3-hydroxy-5-methylisoxazole-4-propionic acid (AMPA) receptor partial agonism. *J. Biol. Chem.* 287: 43557–43564. https://doi.org/10.1074/jbc.M112.371815

Riva, I., C. Eibl, R. Volkmer, A.L. Carbone, and A.J. Plested. 2017. Control of AMPA receptor activity by the extracellular loops of auxiliary proteins. *eLife.* 6:e28680. https://doi.org/10.7554/eLife.28680

Rosenmund, C., Y. Stern-Bach, and C.F. Stevens. 1998. The tetrameric structure of a glutamate receptor channel. *Science.* 280:1596–1599. https://doi.org/10.1126/science.280.5369.1596

Shaikh, S.A., D.M. Dolino, G. Lee, S. Chatterjee, D.M. MacLean, C. Flatebo, C.F. Landes, and V. Jayaraman. 2016. Stargazin modulation of AMPA receptors. *Cell Reports.* 17:328–335. https://doi.org/10.1016/j.celrep.2016.09.014

Shelley, C., M. Farrant, and S.G. Cull-Candy. 2012. TARP-associated AMPA receptors display an increased maximum channel conductance and multiple kinetically distinct open states. *J. Physiol.* 590:5723–5738. https://doi.org/10.1113/jphysiol.2012.238006

Shepherd, J.D., and R.L. Huganir. 2007. The cell biology of synaptic plasticity: AMPA receptor trafficking. *Annu. Rev. Cell Dev. Biol.* 23:613–643. https://doi.org/10.1146/annurev.cellbio.23.090506.123516

Shuang, B., D. Cooper, J.N. Taylor, L. Kisley, J. Chen, W. Wang, C.B. Li, T. Komatsuzaki, and C.F. Landes. 2014. Fast step transition and state identification (STaSI) for discrete single-molecule data analysis. *J. Phys. Chem. Lett.* 5:3157–3161. https://doi.org/10.1021/jz501435p

Sobolevsky, A.I., M.P. Rosconi, and E. Gouaux. 2009. X-ray structure, symmetry and mechanism of an AMPA-subtype glutamate receptor. *Nature.* 462:745–756. https://doi.org/10.1038/nature08624

Stern-Bach, Y., S. Russo, M. Neuman, and C. Rosenmund. 1998. A point mutation in the glutamate binding site blocks desensitization of AMPA receptors. *Neuron.* 21:907–918. https://doi.org/10.1016/S0896-6273(00)80605-4

Sun, Y., R. Olson, M. Horning, N. Armstrong, M. Mayer, and E. Gouaux. 2002. Mechanism of glutamate receptor desensitization. *Nature.* 417:245–253. https://doi.org/10.1038/417245a

Taylor, J.N., and C.F. Landes. 2011. Improved resolution of complex single-molecule FRET systems via wavelet shrinkage. *J. Phys. Chem. B.* 115(5): 1105–1114. . https://doi.org/10.1021/jp1050707

Taylor, J.N., D.E. Makarov, and C.F. Landes. 2010. Denoising single-molecule FRET trajectories with wavelets and Bayesian inference. *Biophys. J.* 98(1):164–173. . https://doi.org/10.1016/j.bpj.2009.09.047

Tomita, S., H. Adesnik, M. Sekiguchi, W. Zhang, K. Wada, J.R. Howe, R.A. Nicoll, and D.S. Bredt. 2005. Stargazin modulates AMPA receptor gating and trafficking by distinct domains. *Nature.* 435:1052–1058. https://doi.org/10.1038/nature03624

Traynelis, S.F., L.P. Wollmuth, C.J. McBain, F.S. Menniti, K.M. Vance, K.K. Ogden, K.B. Hansen, H. Yuan, S.J. Myers, and R. Dingledine. 2010. Glutamate receptor ion channels: structure, regulation, and function. *Pharmacol. Rev.* 62:405–496. https://doi.org/10.1124/pr.109.002451

Twomey, E.C., M.V. Yelshanskaya, R.A. Grassucci, J. Frank, and A.I. Sobolevsky. 2016. Elucidation of AMPA receptor-stargazin complexes by cryo-electron microscopy. *Science.* 353:83–86. https://doi.org/10.1126/science.aaf8411

Twomey, E.C., M.V. Yelshanskaya, R.A. Grassucci, J. Frank, and A.I. Sobolevsky. 2017. Channel opening and gating mechanism in AMPA-subtype glutamate receptors. *Nature.* 549:60–65. https://doi.org/10.1038/nature23479

Yelshanskaya, M.V., M. Li, and A.I. Sobolevsky. 2014. Structure of an agonist-bound ionotropic glutamate receptor. *Science.* 345:1070–1074. https://doi.org/10.1126/science.1256508

Zhang, W., S.P. Devi, S. Tomita, and J.R. Howe. 2014. Auxiliary proteins promote modal gating of AMPA- and kainate-type glutamate receptors. *Eur. J. Neurosci.* 39:1138–1147. https://doi.org/10.1111/ejn.12519

Zhang, W., C. Eibl, A.M. Weeks, I. Riva, Y.J. Li, A.J.R. Plested, and J.R. Howe. 2017. Unitary properties of AMPA receptors with reduced desensitization. *Biophys. J.* 113:2218–2235. https://doi.org/10.1016/j.bpj.2017.07.030

Zhao, Y., S. Chen, C. Yoshioka, I. Baconguis, and E. Gouaux. 2016. Architecture of fully occupied GluA2 AMPA receptor-TARP complex elucidated by cryo-EM. *Nature.* 536:108–111. https://doi.org/10.1038/nature18961

Supplemental material

Carrillo et al., https://doi.org/10.1085/jgp.201912451

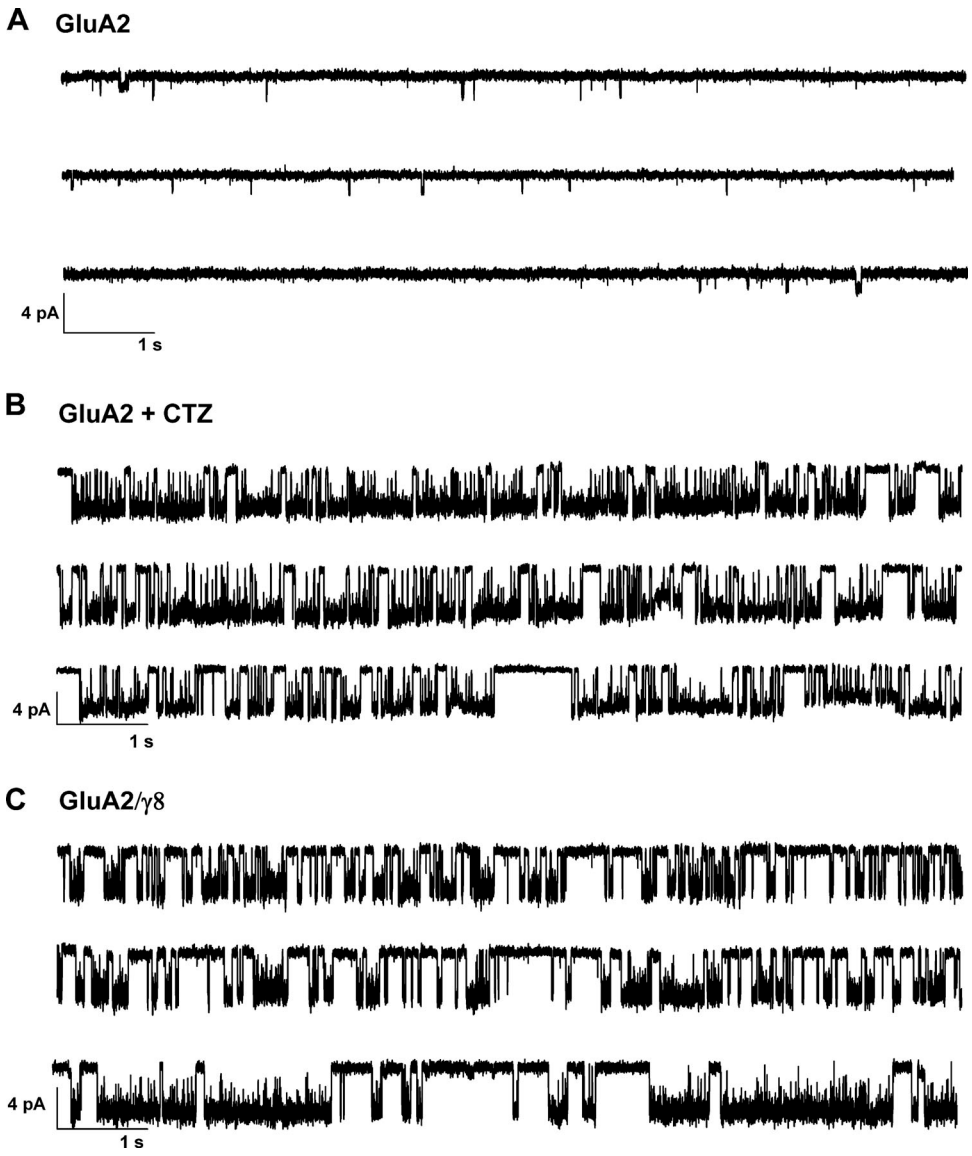

Figure S1. **Representative single-channel currents in cell-attached mode in the presence of 10 mM glutamate (related to Fig. 1).** Each trace is from a different patch and shows variability in different patches.

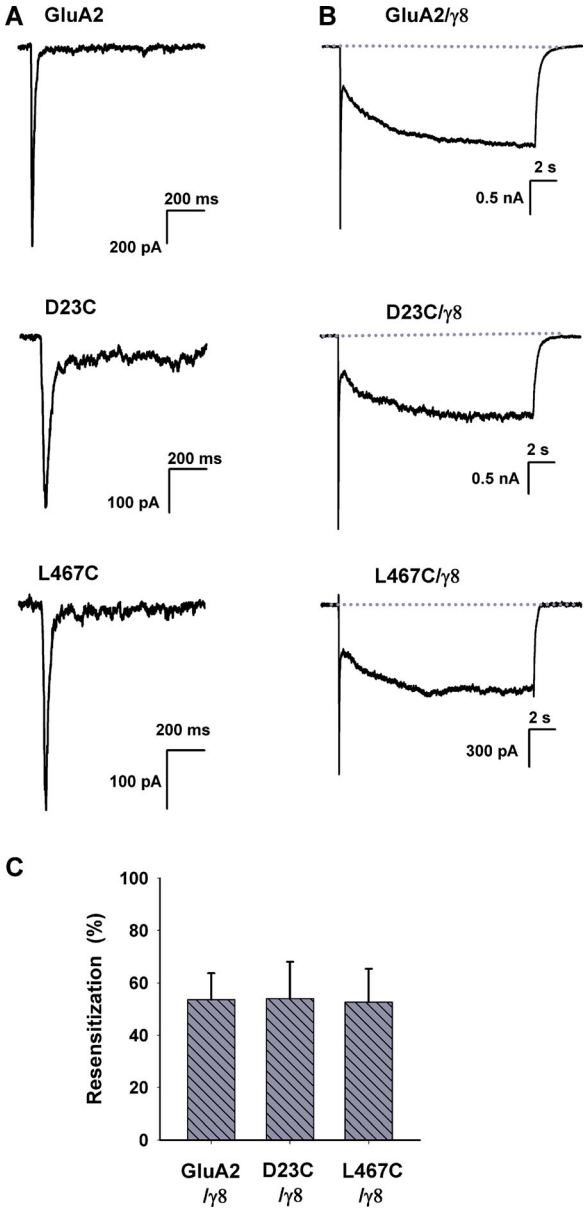

Figure S2. **Representative whole-cell recordings of HEK cells expressing WT GluA2, GluA2-D23C, and GluA2-L467C. (A)** Each receptor alone. **(B)** Each receptor in tandem with γ8. **(C)** Summary data show the percentage resensitization of the constructs in tandem with γ8. Error bars are SEM. Resensitization (%) was quantified as the percentage of the ratio of the steady-state current to the initial peak current response evoked by the application of 10 mM glutamate.

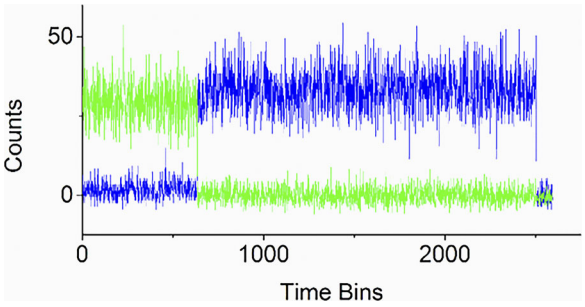

Figure S3. **Representative smFRET trace obtained with donor excitation and detected in the donor and acceptor emission wavelengths.** The trace shows a single photobleaching step for the acceptor (green) and a single photobleaching step for the donor (blue). Only traces showing a single photobleaching step with anticorrelation between the donor and acceptor fluorophores were considered for the smFRET analysis. FRET efficiencies were determined from the donor and acceptor intensities before photobleaching.